Original Article

Biomechanical analysis of atlantoaxial dorsal fixation using finite element models

Beomju Bae[1†] Dongwook Kim[1†] Hyejong Oh[1] Gonhyung Kim[1*]

Abstract

Atlantoaxial instability can cause spinal cord compression with clinical signs ranging from cervical pain to tetraplegia and death. Although a variety of dorsal fixation techniques have been described, some of them have been related to the fracture of the dorsal arch of the atlas, leading to surgical failure. Under the hypothesis that the shape of the dorsal arch of the atlas and types of implants might affect these bone fractures, the objective of this study was to analyze bone stresses through simulations of the dorsal fixation using finite element models. Arbitrary tension forces were given to implants for simulations of the dorsal fixation and the maximum von Mises stress of the bone was analyzed. The maximum bone stress increased as the bone got thinner and the angle of the notch got steeper. The width between wires and the length of the bone did not affect the maximum stress on the bone. Bone with band implant had lower maximum bone stress than that with wire implants. When using wire implants, wires applied beyond the notch of the dorsal arch reduced the maximum bone stress more than wires positioned within it. Therefore, the fracture of the dorsal arch of the atlas was related to the shape of the bone and types of implant applied. Band implant can effectively reduce fracture of the dorsal arch compared to wire implant in atlantoaxial dorsal fixation. When considering wire implant, it is recommended to apply wires beyond the notch of the atlas.

Keywords: atlantoaxial instability, bone fracture, dorsal fixation, finite element model, stress analysis

[1]*Department of Veterinary Surgery, College of Veterinary Medicine, Chungbuk National University, Cheongju 28644, Republic of Korea*

[†]*These authors contributed equally to the work*

***Correspondence**: ghkim@cbu.ac.kr* (G. Kim)

Received October 1, 2021

Accepted February 4, 2022

https://doi.org/10.14456/tjvm.2022.19

Introduction

Atlantoaxial instability (AAI) occurs due to congenital or traumatic causes or a combination of the two. Congenital AAI has been commonly described in immature toy breed dogs. It develops from a loss of atlantoaxial ligamentous support, abnormalities of the dens such as aplasia, hypoplasia, dorsal angulation or nonunion of the ossification center and incomplete ossification of the atlas (Aikawa *et al*., 2013; Sánchez-Masian *et al*., 2014; Riedinger *et al*., 2015). Traumatic AAI can occur at any age in any breed of dog. It usually results from rupture of atlantoaxial ligaments and/or fracture of the dens, although most cases are related to underlying congenital anomalies (Beaver *et al*., 2000; Sanders *et al*., 2004; Riedinger *et al*., 2015). Regardless of the cause, AAI can cause spinal cord compression with clinical signs ranging from cervical pain to tetraplegia and death (Beaver *et al*., 2000; Sanders *et al*., 2004; Pujol *et al*., 2010; Aikawa *et al*., 2013). Treatment of AAI varies from conservative management to surgical stabilization including dorsal and ventral fixation techniques. Conservative management using a cervical splint is a viable option for young dogs with mild or acute clinical signs (Havig *et al*., 2005) but surgical stabilization is recommended for most dogs with AAI because conservative management has the risk of relapse and deterioration (Sanders *et al*., 2004; Stalin *et al*., 2015). Although ventral stabilization by arthrodesis and fusion can provide more rigidity than dorsal stabilization by fibrous tissue formation (Sánchez-Masian *et al*., 2014; Riedinger *et al*., 2015), it is sometimes challenging in toy breed dogs due to their small sized bones, leading to surgical failure (Pujol *et al*., 2010). Thus, various dorsal fixation techniques including the use of wire, dorsal cross pinning with polymethylmethacrylate, nuchal ligament, prosthetic suture material, intermuscular suture and metallic retractor have been described in toy breed dogs (Denny *et al*., 1988; Thomas *et al*., 1991; Jeffery, 1996; Pujol *et al*., 2010; Sánchez-Masian *et al*., 2014). However, some of them have been related to fracture of the dorsal arch of the atlas which can cause surgical failure with subsequence relapse (Thomas *et al*., 1991). Finite element models (FEMs) were introduced into human biomechanics in the early 70s. They have been developed with the continuous advancement of computer technology (Yoganandan *et al*., 1996). Although FEMs have been widely used in human spine biomechanics to analyze fractures (Bozkus *et al*., 2001; Teo and Ng, 2001), injuries (Zhang *et al*., 2011; Hong *et al*., 2014) and surgical techniques (Kim *et al*., 2006; Chun *et al*., 2018), only a few studies have used FEMs in canine spine biomechanics that is known to adapt human material properties (Lim *et al*., 1994; Villarraga *et al*., 1999; Bonelli *et al*., 2018). To the author's knowledge there are very few biomechanical studies for fracture of the dorsal arch of the atlas in atlantoaxial dorsal fixation. Based on our clinical experience that proper positioning of the implant can reduce fracture of the dorsal arch in atlantoaxial dorsal fixation, we hypothesized that the shape of the dorsal arch of the atlas and types of implants might affect the fracture. Thus, the objective of this study was to analyze bone stresses through simulations of the dorsal fixation using FEMs so that we could find a way to reduce bone fracture.

Materials and Methods

Geometric and finite element modeling of bones and implants for simulations of atlantoaxial dorsal fixation and finite element analyses for the bone stresses were performed using Abaqus software program (Abaqus®, Version 6.10; Abaqus, Inc., Providence, RI, USA). This study was approved by the Chungbuk National University Institutional Animal Care and Use Committees (CBNUA-1429-20-01).

Geometric modeling of bones and implants: Bones used in this study were simplified to platy or arch-shaped structures. Arch-shaped bone was modeled based on a three-dimensional (3D) computed tomography (CT) image for the dorsal arch of the atlas of a toy breed dog (a 9-year-old male Maltese dog) without any cervical disease. As the CT image for the dorsal arch of the atlas was obtained from a client-owned dog, informed consent was given by the owner before using the image. The 3D CT image had been taken using a four-row multidetector CT scanner (Hi Speed QX/I; GE Medical Co., Milwaukee, WI, USA) and Medicine (DICOM) viewer (OsiriX MD 4.1.2; OsiriXPixmeo, Geneva, Switzerland). Characteristics of the arch-shaped bone were as follows: 1) the bone got slightly thicker as it went laterally; 2) the bone had a notch with steep oblique angle in the craniomedial part; 3) the bone had cranial protrusions on both sides of the notch; and 4) the lateral part of the bone beyond the notch had a gentle oblique angle. Details for the arch-shaped bone are shown in Fig. 1. Two types of implants (wire implant and band implant) were modeled and applied to the bones. The diameter of the wire implant was 0.8 mm. The thickness of the band implant was also 0.8 mm.

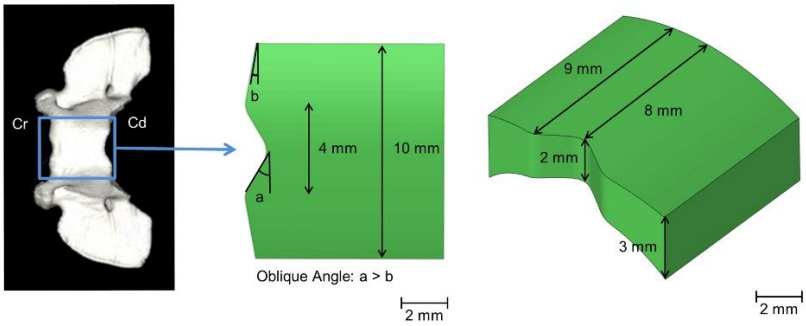

Figure 1 The geometry of an arch-shaped bone based on the dorsal arch of the atlas of a 9-year-old male Maltese dog without any cervical disease (Cr: cranial, Cd: caudal).

Finite element modeling: 3D FEMs for simulations of dorsal fixation were generated using hexahedral and pentahedral elements (Fig. 2). On average, 36,023 nodes and 28,557 elements were used in each simulation. The bones were defined as cortical bones. Cancellous bones in the internal matrix were ignored. Implants were made of stainless steel. The material properties of bones and implants are shown in Table 1. They were assumed to be homogenous and linear isotropic. The friction coefficient value for bone-steel is 0.37 (López-Campos *et al*., 2018). The material properties of the bones were adapted from a previous study of human atlas (Bozkus *et al*., 2001) because of the lack of material definition for canine spine. The material properties of implants were obtained from the literature on stainless steel (Elert, 2004; Zamani and Oyadiji, 2010).

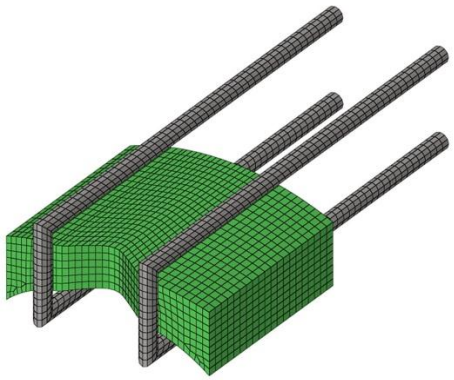

Figure 2 A finite element model representing the arch-shaped bone and wire implants with a width of 6 mm between wires applied for dorsal fixation.

Table 1 Material properties of the bone and the implant (steel) and friction coefficient for steel-bone used in finite element models

	Bone	**Steel**
Elastic modulus (MPa)	10,000	200,000
Poisson's ratio	0.29	0.3
Density (kg/m^3)	40	7700
References	Bozkus *et al*., 2001	Elert, 2004 Zamani and Oyadiji, 2010
	Steel - Bone	
Friction coefficient	0.37	
Reference	López-Campos *et al*., 2018	

Experimental design: Two studies were performed and are referred to as project A and project B. Project A using platy bones was carried out to explain the stress-related results of project B. Project B using arch-shaped bones was implemented to simulate the clinical situation of dorsal fixation.

1. Project A: In project A, influences of various conditions such as bone shapes, implant types and positioning of implants on the platy bones were investigated. Conditions were varied in five models. Model 1 was designed based on the width between wires. Platy bones with a width of 10 mm, a length of 8 mm and a thickness of 1 mm were used and wire implants were applied to the bones. The width between wires was 2 mm in model 1.1, 4 mm in model 1.2 and 6 mm in model 1.3. Model 2 was designed based on the length of the bones. Platy bones with a width of 10 mm and a thickness of 1 mm were used. Wire implants with a width of 4 mm between wires were applied to bones. The length of bones was 8 mm in model 2.1, 9 mm in model 2.2 and 10 mm in model 2.3. Model 3 was designed based on the thickness of bones. Platy bones with a width of 10 mm and a length of 10 mm were used. Wire implants with a width of 6 mm between wires were applied to bones. The thickness of bones was 1 mm in model 3.1, 2 mm in model 3.2 and 3 mm in model 3.3. Model 4 was designed based on the oblique angle of notches. Platy bones with a notch were used. They had a width of 10 mm and a thickness of 1 mm. Wire implants with a width of 4 mm between wires were applied to the oblique planes of notches. The oblique angle was 15° in model 4.1, 30° in model 4.2 and 45° in model 4.3. Model 5 was designed based on types of implants. Platy bones with a width of 10 mm, a length of 10 mm, and a thickness of 2 mm were used. Wire implants with a width of 6 mm between wires and band implant with a width of 6 mm were applied in model 5.1 and model 5.2, respectively (Fig. 3).

2. Project B: In project B, influences of types and positioning of implants on arch-shaped bones were investigated. Four models (referred to as model 6) were used in project B. Wire implants were applied within notches of arch-shaped bones in models 6.1 and 6.2 and beyond the notch in model 6.3. The width between wires was 2 mm in model 6.1, 4 mm in model 6.2 and 6 mm in model 6.3. Band implant with a width of 6 mm was applied in model 6.4 (Fig. 4).

Finite element analyses: Arbitrary tension forces of 20 Newtons (N) were applied to implants in project A while 20 N, 40 N and 80 N of tension forces were applied to implants in project B for simulations of the dorsal fixation. The maximum bone stresses under these forces did not exceed the yield stress of cortical bone. Considering our bone elastic modulus [10 gigapascal (GPa)], the bone yield stress in this study was 66.4 megapascal (MPa) [yield stress (MPa) = 24.4 + 4.20 × elastic modulus (GPa)] (Bayraktar *et al*., 2004). If the maximum bone stress gets close to the yield stress, the bone will be vulnerable to bone fracture. The maximum von Mises stress in the bone for each model was measured and compared to each other to find out which models had lower maximum stresses.

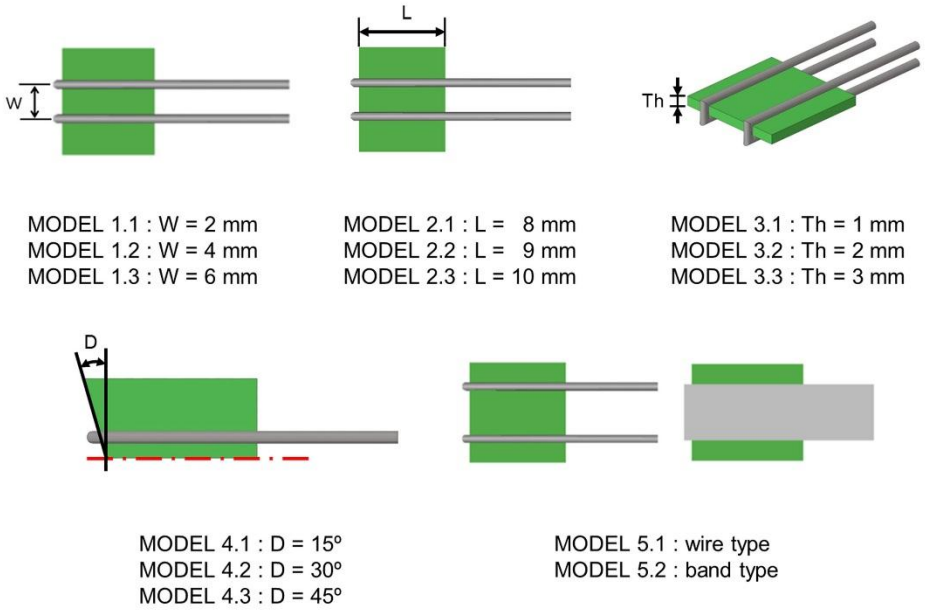

Figure 3 Project A (models 1-5) using platy bones under various conditions. Models were designed based on the width between wires in model 1, the length of bones in model 2, the thickness of bones in model 3, the oblique angle of notches in model 4 and types of implants in model 5 (W: width, L: length, Th: thickness, D: oblique angle).

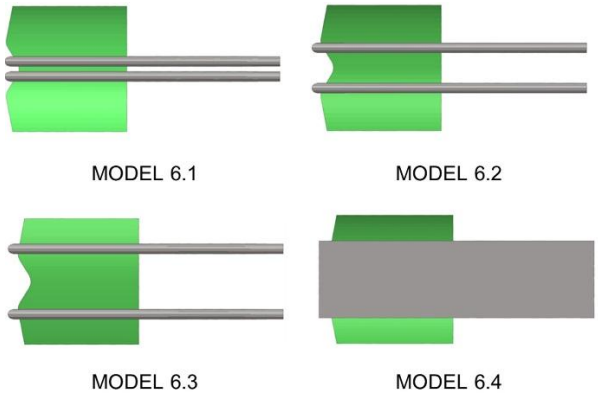

Figure 4 Project B (model 6) using arch-shaped bones designed based on types and positioning of implants. Wire implants were applied within notches of arch-shaped bones in models 6.1 and 6.2. They were applied beyond the notch in model 6.3. The band implant was applied in model 6.4.

Results

1. Project A: The maximum von Mises stress related to the width (W) between wires was 21.276 MPa in model 1.1 (W = 2 mm), 20.798 MPa in model 1.2 (W = 4 mm) and 20.851 MPa in model 1.3 (W = 6 mm). In model 2 related to the length (L) of the bones, the maximum von Mises stress was 20.798 MPa in model 2.1 (L = 8 mm), 20.793 MPa in model 2.2 (L = 9 mm) and 20.790 MPa in model 2.3 (L = 10 mm). The width between wires and the length of the bone did not greatly affect the maximum bone stress. The maximum bone stress increased as the thickness (Th) of the bones decreased. The maximum von Mises stress was 20.845 MPa in model 3.1 (Th = 1 mm), 14.674 MPa in model 3.2 (Th = 2 mm) and 9.158 MPa in model 3.3 (Th = 3 mm). As the oblique angle (D) of the notch increased from 15° to 45°, the maximum bone stress also increased [25.954 MPa in model 4.1 (D = 15°), 34.904 MPa in model 4.2 (D = 30°), and 40.978 MPa in model 4.3 (D = 45°)]. Band implant reduced the maximum bone stress (4.481 MPa in model 5.2) more than wire implant (14.674 MPa in model 5.1) (Table 2).

Table 2 The maximum von Mises stresses under tension force of 20 Newton in models 1-5

Model 1	Width (mm)	2	4	6
	Maximum von Mises stress (MPa)	21.276	20.798	20.851
Model 2	Length (mm)	8	9	10
	Maximum von Mises stress (MPa)	20.798	20.793	20.790
Model 3	Thickness (mm)	1	2	3
	Maximum von Mises stress (MPa)	20.845	14.674	9.158
Model 4	Oblique angle (°)	15	30	45
	Maximum von Mises stress (MPa)	25.954	34.904	40.978
Model 5	Types of implants	Wire	Band	
	Maximum von Mises stress (MPa)	14.674	4.481	

MPa, megapascal

2. *Project B:* The maximum bone stresses were 15.207 MPa under 20 N, 29.067 MPa under 40 N and 50.231 MPa under 80 N in model 6.1. In model 6.2, the maximum bone stresses were 13.695 MPa under 20 N, 23.584 MPa under 40 N, and 40.557 MPa under 80 N. In model 6.3 with wires applied beyond the notch, the maximum bone stresses were 10.748 MPa under 20 N, 16.333 MPa under 40 N and 27.452 MPa under 80 N. Thus, wires applied within notches of arch-shaped bones increased the maximum bone stress more than wires positioned beyond the notch. In model 6.4 using band implant showed the maximum bone stresses of 9.591 MPa under 20 N, 13.006 MPa under 40 N and 23.944 MPa under 80 N. When using band implant, the maximum bone stress decreased compared to that when wire implants were used. Under tension forces of 20 N, 40 N and 80 N, differences in maximum bone stresses between model 6.3 and model 6.4 were 1.157 MPa, 3.327 MPa, and 3.508 MPa, respectively. Under the forces of 20 N, 40 N and 80 N, differences in maximum bone stresses between model 6.1 and model 6.4 were 5.616 MPa, 16.061 MPa, and 26.287 MPa, respectively. As the force increased from 20 N to 80 N, the difference in the maximum bone stress between model 6.1 and model 6.4 (20.671 MPa) increased much more than that between model 6.3 and model 6.4 (2.351 MPa). Under the force of 80 N, the maximum bone stresses in models 6.1 and 6.2 were relatively closer to the bone yield stress than those in models 6.3 and 6.4 (Fig. 5 and Fig. 6).

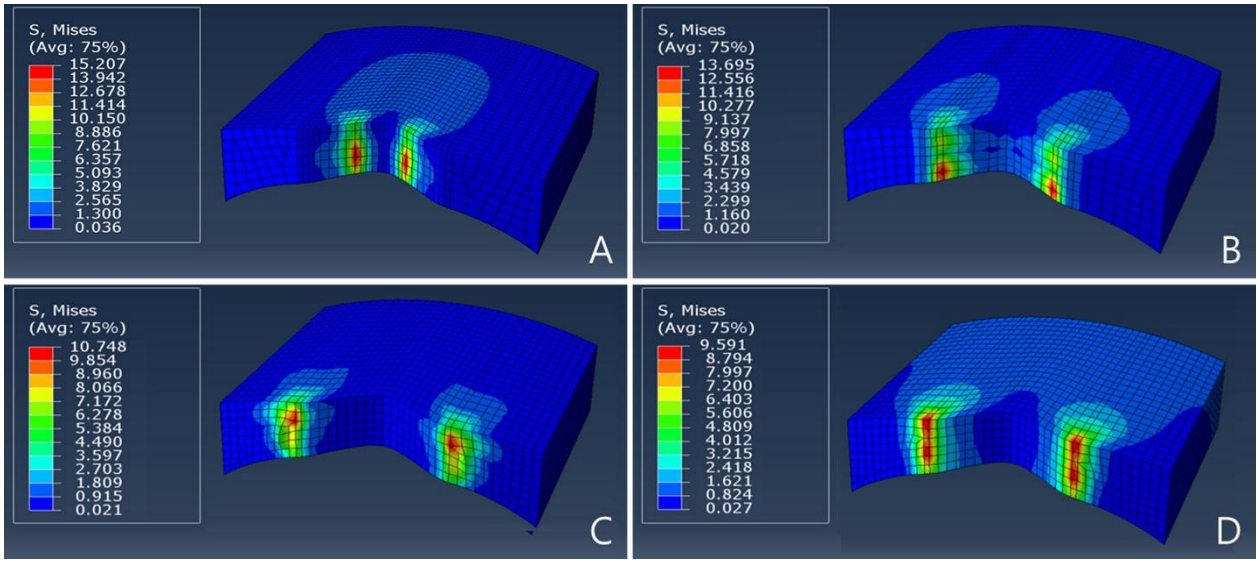

Figure 5 Von Mises stress distribution in arch-shaped bones according to the type and positioning of the implant (model 6). Wire implants were applied within notches in models 6.1 (A) and 6.2 (B). A wire implant was applied beyond the notch in model 6.3 (C). A band implant was applied in model 6.4 (D).

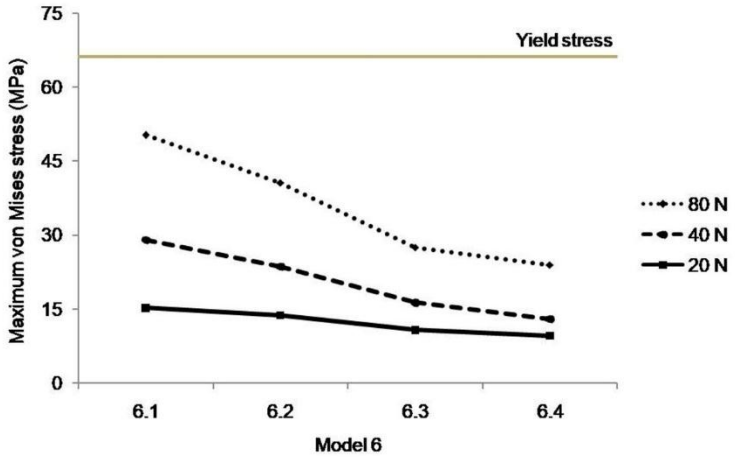

Figure 6 The maximum von Mises stresses under tension forces of 20 N, 40 N, and 80 N in model 6. Wire implants were applied within notches in models 6.1 and 6.2. A wire implant was applied beyond the notch in model 6.3. A band implant was applied in model 6.4.

Discussion

Models for biomechanical study such as in vitro, in vivo and FEMs have greatly improved our understanding of biomechanics and medicine (Panjabi, 1998). FEMs can evaluate internal response such as stress-related information which is difficult to obtain in in vivo and in vitro models (Brolin and Halldin, 2004; Zhang *et al*., 2005). Stress analysis is important to understand the fracture mechanism. Thus, FEMs have been widely used for studies on bone fractures (Lotz *et al*., 1991; Bozkus *et al*., 2001; Teo and Ng, 2001; Rodrigues *et al*., 2012). We modeled the arch-shaped bone reflecting characteristics of the dorsal arch of the canine atlas and analyzed the behavior of the spinal bone fracture in atlantoaxial dorsal fixation using FEMs. In patients with AAI, ligamentous lesions such as disruption of atlantoaxial ligaments, osseous lesions such as dens fracture or a combination of them cause distraction of the atlantoaxial joint related to atlantoaxial subluxation (Deliganis *et al*., 2000; Meyer *et al*., 2019). Thus, we applied tension forces to implants for simulations of atlantoaxial dorsal fixation which handles the distraction force. When giving tension forces to implants, the maximum bone stress increased as bone got thinner and the oblique angle got steeper. Considering the shape of the dorsal arch of the canine atlas which has a thin notch with steep oblique angle, the bone will get greater maximum stress if the implant is applied to this notch during dorsal fixation. In the arch-shaped bone based on atlas, the maximum bone stress was actually higher and closer to bone yield stress when applying wires within the notch compared to that when positioning them laterally beyond the notch. In addition, as tension force to the implant increased, difference in the maximum bone stress between the bone with wires applied within the notch and the bone with them positioned beyond the notch also increased. Thus, the bone with wires positioned beyond the notch is less vulnerable to bone fracture than the bone with wires applied within it. One clinical study on dorsal stabilization for dogs with AAI has reported that fracture of the dorsal arch is reduced with the use of band implant due to an increased contact surface between the bone and the implant, leading to better repartition of forces (Pujol *et al*., 2010). If the bone is flat and platy, band implant can reduce the maximum bone stress effectively compared to wire implants. However, the dorsal arch of the canine atlas has protrusions that can prevent band implant from reducing the maximum bone stress as the decreased contact surface can lead to higher concentrations of the stress. In our study, the reduction of the maximum bone stress by band implant in arch-shaped bone (1.157 MPa) was less than that in the platy bone (10.193 MPa) under 20 N of the force. In addition, when the tension force to implants increased from 20 N to 80 N, the difference in the maximum bone stress between the bone with wires positioned beyond the notch and the bone with band implant was increased by only 2.351 MPa while that between the bone with wires applied within the notch and the bone with the band implant was increased by 20.671 MPa. Taken together, although a band implant can reduce the maximum bone stress and the risk of bone fracture compared to wire implants, wire implants can also decrease the risk of bone fracture if the wires are applied beyond the notch. Several limitations to our models exist. Although the shape of the atlas might vary between breeds (Parry *et al*., 2010), there was no consideration for individual or breed variation during the modeling of the dorsal arch. However, characteristics reflected in our arch-shaped bone model can be applied to the dorsal arches of most toy breed dogs. In performing the study, the material properties for human were used due to the lack of those for canines. No significant issue has been reported in studies on canine spine using human material properties (Bonelli *et al*., 2018) but further studies are needed to set proper material properties for a more realistic behavior of canine bone model and to validate FEMs in canine study. Although spine response is nonlinear, linear analysis related to distraction force was conducted in this study. This is because linear models could make analysis simpler and have been successfully used to understand bone fractures in previous studies (Lotz *et al*., 1991; Whyne *et al*., 1998; Teo and Ng, 2001). In addition to distraction force, other forces such as flexion, extension, shear force, lateral bending and axial rotation are also possible in atlantoaxial joints and should be further

considered. In conclusion, these results showed that the fracture of the dorsal arch was closely associated with bone shape and types of implants. Band implant reduced the maximum bone stress the most. When using wire implants, consideration for the thickness and inclination of the atlas is necessary to decrease the maximum stress in the bone.

Acknowledgements

The authors thank Hyunhee Lee (MS in Engineering) at Korea University of Technology and Education for providing technical support. Korea Institute for Robot Industry Advancement supplied the software used for analysis.

References

Aikawa T, Shibata M and Fujita H 2013. Modified ventral stabilization using positively threaded profile pins and polymethylmethacrylate for atlantoaxial instability in 49 dogs. Vet Surg. 42: 683-692.

Bayraktar HH, Morgan EF, Niebur GL, Morris GE, Wong EK and Keaveny TM 2004. Comparison of the elastic and yield properties of human femoral trabecular and cortical bone tissue. J Biomech. 37: 27-35.

Beaver DP, Ellison GW, Lewis DD, Goring RL, Kubilis PS and Barchard C 2000. Risk factors affecting the outcome of surgery for atlantoaxial subluxation in dogs: 46 cases (1978-1998). J Am Vet Med Assoc. 216: 1104-1109.

Bonelli MA, Shah A, Goel V, Costa FS and da Costa RC 2018. Development of a finite element model of the ligamentous cervical vertebral column of a Great Dane. Res Vet Sci. 118: 97-100.

Bozkus H, Karakas A, Hanci M, Uzan M, Bozdag E and Sarioglu AC 2001. Finite element model of the Jefferson fracture: comparison with a cadaver model. Eur Spine J. 10: 257-263.

Brolin K and Halldin P 2004. Development of a finite element model of the upper cervical spine and a parameter study of ligament characteristics. Spine (Phila Pa 1976). 29: 376-385.

Chun DH, Yoon DH, Kim KN, Yi S, Shin DA and Ha Y 2018. Biomechanical comparison of four different atlantoaxial posterior fixation constructs in adults: a finite element study. Spine (Phila Pa 1976). 43: E891-E897.

Deliganis AV, Baxter AB, Hanson JA, Fisher DJ, Cohen WA, Wilson AJ and Mann FA 2000. Radiologic spectrum of craniocervical distraction injuries. Radiographics. 20: S237-S250.

Denny HR, Gibbs C and Waterman A 1988. Atlanto-axial subluxation in the dog: a review of thirty cases and an evaluation of treatment by lag screw fixation. J Small Anim Pract. 29: 37-47.

Elert G 2004. Density of Steel. http://hypertextbook.com/facts/2004/KarenSutherland.shtml.

Havig ME, Cornell KK, Hawthorne JC, McDonnell JJ and Selcer BA 2005. Evaluation of nonsurgical treatment of atlantoaxial subluxation in dogs: 19 cases (1992-2001). J Am Vet Med Assoc. 227: 257-262.

Hong JT, Qasim M, Orias AAE, Natarajan RN and An HS 2014. A biomechanical comparison of three different posterior fixation constructs used for c6–c7 cervical spine immobilization: a finite element study. Neurol Med Chir (Tokyo). 54: 727-735.

Jeffery ND 1996. Dorsal cross pinning of the atlantoaxial joint: new surgical technique for atlantoaxial subluxation. J Small Anim Pract. 37: 26-29.

Kim HS, Kim YS and Mun JH 2006. Moment prediction for evaluating stability of the upper cervical spine fixed with wires using finite element analysis. Key Eng Mater. 321-323: 1098-1102.

Lim TH, Goel VK, Weinstein JN and Kong W 1994. Stress analysis of a canine spinal motion segment using the finite element technique. J Biomech. 27: 1259-1269.

López-Campos JA, Segade A, Casarejos E, Fernández JR, Vilán JA and Izquierdo P 2018. Finite element study of a threaded fastening: the case of surgical screws in bone. Symmetry. 10: 335.

Lotz JC, Cheal EJ and Hayes WC 1991. Fracture prediction for the proximal femur using finite element models: part I--linear analysis. J Biomech Eng. 113: 353-360.

Meyer C, Eysel P and Stein G 2019. Traumatic atlantoaxial and fracture-related dislocation. Biomed Res Int. 2019: 5297950.

Panjabi MM 1998. Cervical spine models for biomechanical research. Spine (Phila Pa 1976). 23: 2684-2700.

Parry AT, Upjohn MM, Schlegl K, Kneissl S and Lamb CR 2010. Computed tomography variations in morphology of the canine atlas in dogs with and without atlantoaxial subluxation. Vet Radiol Ultrasound. 51: 596-600.

Pujol E, Bouvy B, Omaña M, Fortuny M, Riera L and Pujol P 2010. Use of the Kishigami atlantoaxial tension band in eight toy breed dogs with atlantoaxial subluxation. Vet Surg. 39: 35-42.

Riedinger B, Bürki A, Stahl C, Howard J and Forterre F 2015. Biomechanical evaluation of the stabilizing function of three atlantoaxial implants under shear loading: a canine cadaveric study. Vet Surg. 44: 957-963.

Rodrigues LB, Las Casas EB, Lopes DS, Folgado J, Fernandes PR, Pires EA, Alves GE and Faleiros RR 2012. A finite element model to simulate femoral fractures in calves: testing different polymers for intramedullary interlocking nails. Vet Surg. 41: 838-844.

Sánchez-Masian D, Luján-Feliu-Pascual A, Font C and Mascort J 2014. Dorsal stabilization of atlantoaxial subluxation using non-absorbable sutures in toy breed dogs. Vet Comp Orthop Traumatol. 27: 62-67.

Sanders SG, Bagley RS, Silver GM, Moore M and Tucker RL 2004. Outcomes and complications associated with ventral screws, pins, and polymethyl methacrylate for atlantoaxial instability in 12 dogs. J Am Anim Hosp Assoc. 40: 204-210.

Stalin C, Gutierrez-Quintana R, Faller K, Guevar J, Yeamans C and Penderis J 2015. A review of canine

atlantoaxial joint subluxation. Vet Comp Orthop Traumatol. 28: 1-8.
Teo EC and Ng HW 2001. First cervical vertebra (atlas) fracture mechanism studies using finite element method. J Biomech. 34: 13-21.
Thomas WB, Sorjonen DC and Simpson ST 1991. Surgical management of atlantoaxial subluxation in 23 dogs. Vet Surg. 20: 409-412.
Villarraga ML, Anderson RC, Hart RT and Dinh DH 1999. Contact analysis of a posterior cervical spine plate using a three-dimensional canine finite element model. J Biomech Eng. 121: 206-214.
Whyne CM, Hu SS, Klisch S and Lotz JC 1998. Effect of the pedicle and posterior arch on vertebral body strength predictions in finite element modeling. Spine (Phila Pa 1976). 23: 899-907.
Yoganandan N, Kumaresan S, Voo L and Pintar FA 1996. Finite element applications in human cervical spine modeling. Spine (Phila Pa 1976). 21: 1824-1834.
Zamani AR and Oyadiji SO 2010. Theoretical and finite element modeling of fine Kirschner wires in Ilizarov external fixator. J Med Device. 4: 031001.
Zhang JG, Wang F, Zhou R and Xue Q 2011. A three-dimensional finite element model of the cervical spine: an investigation of whiplash injury. Med Biol Eng Comput. 49: 193-201.
Zhang QH, Teo EC and Ng HW 2005. Development and validation of a C0-C7 FE complex for biomechanical study. J Biomech Eng. 127: 729-735.